PAPER • OPEN ACCESS

Development and prototyping of SMA-metamaterial biaxial composite actuators

View the article online for updates and enhancements.

Development and prototyping of SMA-metamaterial biaxial composite actuators

Luke Mizzi*, Seyedeh Farzaneh Hoseini, Marco Formighieri and Andrea Spaggiari

Dipartimento di Scienze e Metodi dell'Ingegneria, Università di Modena e Reggio Emilia, Reggio Emilia, Italy

E-mail: luke.mizzi@unimore.it

CrossMark

Abstract

Shape memory alloys (SMA) are excellent candidates for implementation in actuator systems due to their ability to recover their original shape after high-strain loading through a thermally-induced phase transition. In this work, we propose and develop a novel SMA-metamaterial actuator which is capable of exhibiting a reversible, global elongation in multiple directions induced by the unidirectional contraction upon heating of a single SMA component. This actuator consists of (a) an SMA component, (b) a bias component and (c) the metamaterial geometry, with each component having a distinct function: (a) actuation activation, (b) reversibility of actuation upon deactivation and (c) amplifying and re-directing the uni-directional SMA actuation globally throughout the actuator, respectively. A prototype actuator was designed and tested in various configurations over multiple activation/deactivation cycles in order to demonstrate the functionality and reusability of this system. Furthermore, a theoretical model which predicts the actuation stroke of the system on the basis of the material properties of the SMA and bias components as well as the geometry of the metamaterial system was developed and validated. The findings of this work demonstrate the considerable potential of SMA-metamaterial actuators for implementation in systems requiring a multi-axial actuation output.

Keywords: shape memory alloys, mechanical metamaterials, actuators, auxetic, composites

(Some figures may appear in colour only in the online journal)

1. Introduction

Shape memory alloys (SMAs) are materials which have the ability to recover their original shape after loading through a thermally-induced crystallographic phase transition from a martensitic to an austenitic state [1–3]. This remarkable property makes them particularly well-suited for implementation in actuators since the shape memory effect is functional over a considerable strain range (*ca*. 2%–5% strain) and is also characterised by a high force to stroke ratio [4]. The most commonly-used SMA in the field of actuation is Nitinol; a commercial name for a nickel titanium alloy which apart from its shape memory behaviour also exhibits superelasticity in its austenitic phase [5–9]. Although the phase transition temperatures of this alloy can be varied by altering the mixing ratios of its constituent elements, Nitinol is normally in the martensitic phase at room temperature and typically undergoes thermal

---

* Author to whom any correspondence should be addressed.

hysteresis between the martensite and austenite phases at a temperature range of 20–50 K.

Since the implementation of SMAs in actuators [10–13] requires the application of a pre-strain, a stand-alone one-way SMA-based actuator is only suitable for one-time use as once the actuator is heated it reverts to its original state and the initial level of pre-strain is not re-applied upon cooling. In order to avoid this design problem and impart reusability to the actuator, a so-called 'bias' mechanism is incorporated into the actuator which counterbalances the actuation of the SMA component and returns it to its initial pre-strain state once the actuator is deactivated. The bias component imparts reversibility to the actuator by taking advantage of the differences in Young's modulus between martensitic and austenitic phases (with the latter being the stiffer of the two). The counterbalance component should ideally ensure that the SMA component is at its maximal level of recoverable pre-strain in its cold-phase while exerting the least amount of resistance to the SMA contraction upon heating [14]. This delicate balancing act between these two opposing factors is highly dependent on the relative stiffnesses, volume fractions and type of mechanical interaction between the SMA and bias component and careful consideration must be given at the design stage to these aspects in order to ensure that the optimal stroke and/or force output is obtained.

A number of studies may be found in the literature regarding the design, fabrication and implementation of SMA-based bias actuators in various applications [15]. The SMA component is typically employed in the form of a wire, strip or spring, with the former two favouring high-force applications and the latter systems requiring a large stroke output. On the other hand, the bias component can be integrated in the form of a fixed weight, springs, deformable elastic block of material, a flexing beam or even a second, opposing SMA component [16–27]. Furthermore, the actual actuation stroke/force of the actuator need not necessarily act in the same direction as the contraction of the SMA component upon heating. It is possible to change the direction of actuation, enhance the resultant stroke and even obtain an overall elongation output instead of a contraction by mechanical design. One of the most well-known examples of such an actuator is the SMA-sandwich actuator, where the SMA component is integrated into the faces of a sandwich structure with a soft core and selective activation of the SMA component on one surface results in a tailorable flexural deformation that induces elongation of the actuator in the direction orthogonal to the contraction of the SMA component [28–34]. The resultant elongation stroke imparted by such a system can exceed considerably the actual contraction of the SMA component, but the enhanced stroke comes at the cost of a significant reduction in actuation force in the same direction.

In this work, we propose a novel SMA-based actuator which takes this concept further and is capable of exhibiting a reversible, global elongation in multiple directions induced by the unidirectional contraction upon heating of a single SMA component. This actuator incorporates a metamaterial geometry coupled with a SMA and a bias component and takes advantage of the negative Poisson's ratio and particular

kinematic deformation mode of the metamaterial to generate a uniform controllable force/stroke output in both the axial and transverse directions. We have designed and assembled a fully-functional prototype of this actuator using additive manufacturing technology and commercially bought components and tested it under various loading conditions. In addition, we have also developed and validated a theoretical model which may be used to predict the actuation output of the metamaterial actuator based on the geometric parameters of the system and the material properties of the individual components.

2. Design of the SMA-metamaterial actuator

The SMA-metamaterial actuator proposed in this work is based on the rotating squares auxetic metamaterial geometry and is designed to exhibit an elongation stroke concurrently in both the *x*- and *y*-directions upon activation. The rotating squares system [35], shown in figure 1, is one of the most well-known geometries with the ability to exhibit a negative Poisson's ratio and belongs to a class of auxetic metamaterials known as rotating rigid unit systems. These systems include rotating rectangles [36, 37], rhombi [38], parallelograms [39, 40] and triangles [41, 42] among others, as well as 3D rotating polyhedral [43, 44] and have the potential to exhibit giant negative as well as large positive Poisson's ratios. Like all classes of mechanical metamaterials, the mechanical properties of these systems are almost entirely dependent on their structure and can be tailored as a function of the geometric parameters.

The rotating squares metamaterial, as its name implies, deforms through the rotation of squares that are connected to each other at the vertices through pin-joints (in the mechanism's idealised state) [35] or through a thin strip/block of material (in a single-material perforated metamaterial system) [45–48]. It exhibits an in-plane Poisson's ratio of −1 which means that any elongation or contraction in one direction upon loading is accompanied by an identical strain in the transverse direction. In addition, as a pin-joint mechanism, the rotating squares geometry has also been shown to be completely unaffected by edge effects and deforms in the same manner in a periodic infinite, large-scale finite and small-scale finite environment. These two factors make it particularly well-suited for implementation in a biaxial actuation system.

In order to induce a global expansion of the actuator upon activation, it is first necessary to select the correct position for insertion of the pre-strained SMA component, which undergoes contraction upon heating. The deformation of the idealised rotation square system may be expressed in terms of the change in the angle between the square units, θ and this variable governs both the internal localised deformations of the structure and the resultant global strains. As shown in figure 1, the SMA component must be inserted between the points marked A and B since a decrease in the distance between these two points, l_{AB}, upon rotation of the squares induces an expansion of the metamaterial system. Therefore, to quantify the relationship between the internal unit cell lengths l_{AB} and l_{CD} and the global lengths in the *x*- and *y*-directions, denoted by
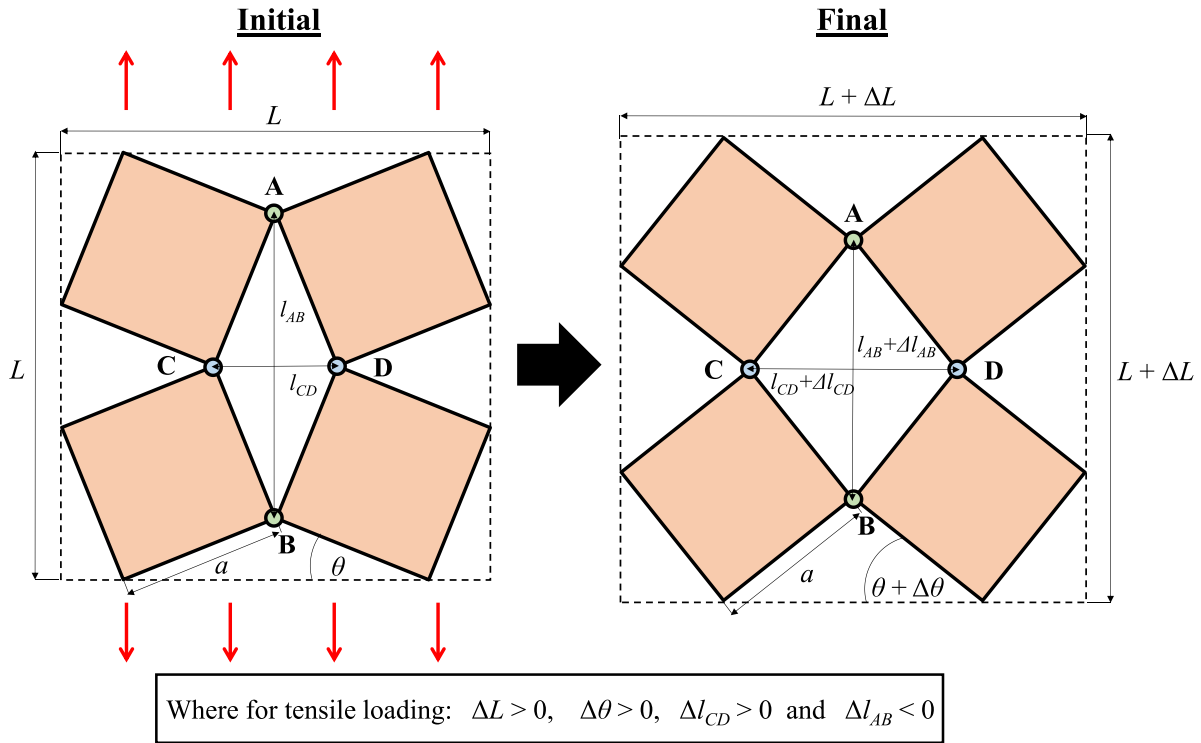
Figure 1. Schematic of a rotating square metamaterial unit cell before and after tensile loading.

the L, these variables must be expressed in terms of the internal angle between squares, θ, and the side length of the squares, a. The following terms may be obtained:

$$L = 2a\left[\sin(\theta) + \cos(\theta)\right] \quad (1)$$

$$l_{AB} = 2a\cos(\theta) \quad (2)$$

$$l_{CD} = 2a\sin(\theta) \quad (3)$$

Since deformation occurs through a change in θ while the side length of the squares, a, remains constant, the relative changes in these three lengths once the metamaterial deforms may be expressed in terms of $\Delta\theta$. An example is plotted in figure 2, where the relative lengths L/a, l_{AB}/a and l_{DC}/a.

As one may observe, the resultant plot is axi-symmetric and the system has one fully-opened configuration at $\theta = 45°$ where $L/a = 2.828$ and two fully closed configurations at $\theta = 0°$ and $\theta = 90°$ where $L/a = 2$. It is also evident that in order to have an inversely-proportional relationship between the lengths L and l_{AB}, the angle θ must be between $0°$ and $45°$. Furthermore, this relationship is nonlinear, and it is clear that at low θ values, a small decrease in the length l_{AB} results in the largest relative increase in L.

3. Theoretical model

Before a prototype SMA-metamaterial actuator based on this concept can be produced, it is necessary to first develop analytical expressions which may be used to predict the actuation output of the system as a function of the material properties

of the individual components and the overall geometry of the system. As stated in the previous section, this actuator consists of three components: the SMA, the bias component and the metamaterial geometry; each of which has a distinct role to play in ensuring the overall functionality of the composite system. The SMA component induces the actuation of the system, the bias component imparts reversibility upon deactivation and reusability to the actuator, and the metamaterial geometry controls the actuation stroke and force output of the system in the axial and transverse directions. These three components are shown in figure 3, where in order to maximise the actuation stroke output, the SMA component is placed in position l_{AB} and the bias component in position l_{CD}. This means that, as illustrated in figure 2, the contraction of the SMA component upon activation is counteracted by an elongation of the bias component imposed through the kinematic constraints of the rotating squares metamaterial deformation mode. Since $l_{AB} > l_{CD}$, this also induces an overall positive actuation stroke of the actuator, i.e. L increases.

In order to quantify the actuation stroke of the system, it is necessary to equilibrate the forces and displacements of the SMA and bias component along the direction l_{AB}. Since the SMA component is aligned along l_{AB}, the force-displacement plot obtained from uniaxial loading of this component can be used directly, as shown in figure 3 (green and red lines). However, this is not the case for the bias component, which is oriented in a direction perpendicular to l_{AB}. Therefore, the forces and displacements exerted by the bias component in the direction l_{AB}, which are necessary to equilibrate the system, must first be found through the kinematic laws that define the deformation of the metamaterial system.
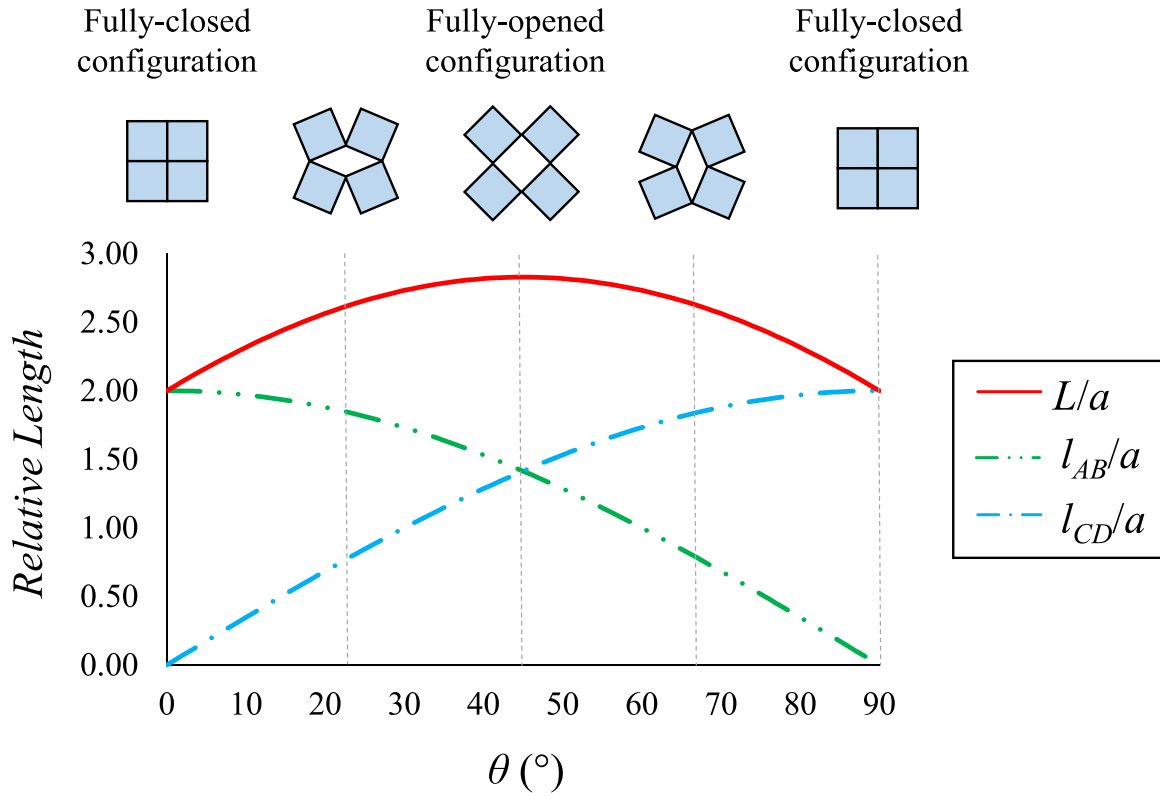
Figure 2. Plot showing the variation in relative lengths L/a, l_{AB}/a and l_{CD}/a upon varying the angle θ.
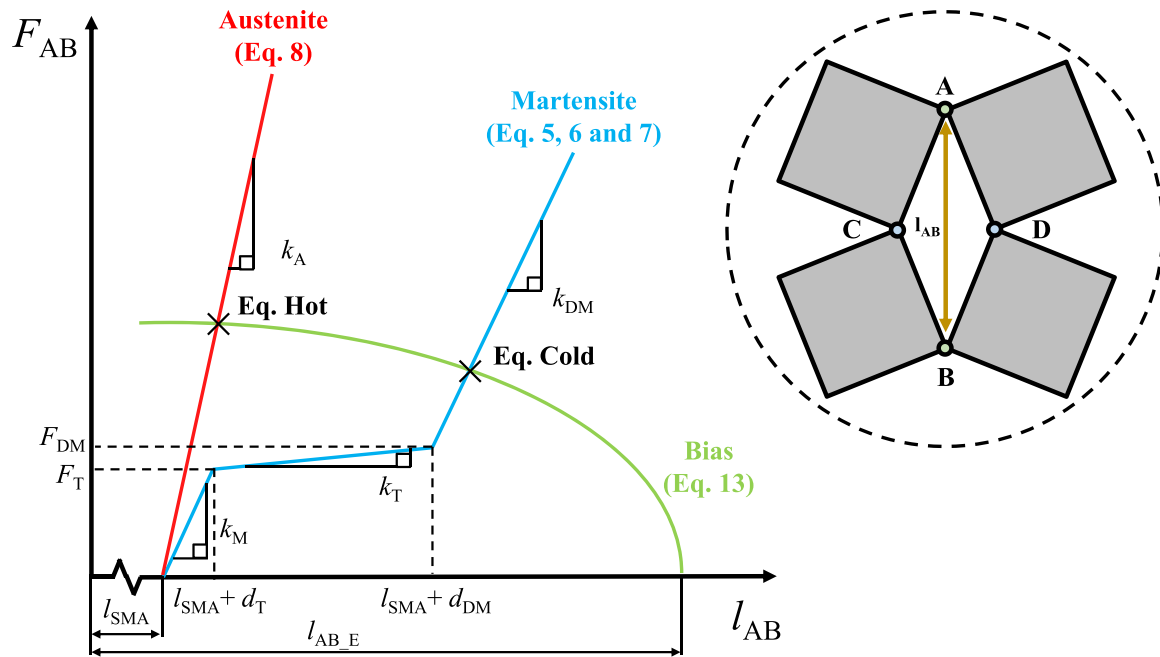

Figure 3. A qualitative plot showing the forces and displacements acting along l_{AB} for the SMA in martensitic (blue) and austenitic state (red) and the opposing bias component (green). The equilibrium points at the SMA hot and cold states are also indicated.

3.1. Assumptions

The model, which predicts the actuation output of the system on the basis of the equilibrium of forces generated by the interaction between the SMA and bias component, is based on a number of assumptions, listed below:

- The metamaterial geometry exerts a solely kinematic influence on the deformation of the overall system and does not contribute any internal energy in terms of work done to the actuator. This means that the influence of factors such as friction at the joints of rotating units and weight is considered to be negligible.

- The stress–strain behaviour of the SMA component at the martensitic phase can be represented in terms of a tri-linear model with each line representing the twinned martensite state (M), transition state (T) and detwinned martensitic state (DM), respectively (see figure 3). On the other hand, the austenitic state is represented by a linear model. This approach is consistent with that utilised in previous works found in the literature pertaining to analytical and numerical analyses of SMAs [14, 49–51].
- Upon activation/heating, the SMA component undergoes a complete transition from martensitic to austenitic phase. This is typically the case for SMA systems with a small cross-sectional area such as wires and strips activated through the Joule effect.
- The model is static and, hence, the deformation of both the SMA and bias component is elastic, fully recoverable and unaffected by the velocity of activation (transformation from martensitic to austenitic phase is almost instantaneous once activated through the use of an electrical current).

The pre-strain of the SMA component is also fully induced by the elastic bias component, which in this case was assumed to be an elastomer or a spring which deforms linearly over high strains. This means that during the assembly of the actuator, the SMA component should ideally be introduced first within the system at a predetermined length, l_{SMA}, followed by the insertion of the elastic bias component. In order for the bias component to exert a pre-stress on the SMA component, the initial length at rest of the bias component, l_E, must be less than the length l_{CD} which corresponds to the length l_{AB} of the SMA component. This condition may be expressed as follows:

$$l_E < \sqrt{4a^2 - l_{l_{\text{SMA}}}^2} \tag{4}$$

and it ensures that the pre-strain applied to the bias component in order to integrate it within the actuator imparts sufficient force to counterbalance the SMA and induces a pre-strain in the latter component.

At this point, it is important to note that although the bias component deforms axially in a linear elastic manner, the fact that it is placed in a position which is perpendicular to the SMA component, means that the equilibrating force induced by the bias component in the direction l_{AB} is nonlinear and kinematically dependent on the metamaterial geometry used. Thus, in figure 3, the force-displacement plot of the bias component along l_{AB} is represented by a nonlinear curve.

3.2. Geometry-force calculations

As stated previously, the force-displacement relationship of the SMA component in its martensitic phase is represented by a tri-linear model. The SMA has an initial length of l_{SMA} at rest and the model (shown in figure 3) may be expressed in terms of force (F_{AB}) and total length (l_{AB}) along the line between the points A and B as follows:

$$F_{AB} = k_{\text{M}}(l_{AB} - l_{\text{SMA}}), \text{ where } l_{\text{SMA}} \leqslant l_{AB} < (l_{\text{SMA}} + d_{\text{T}}) \tag{5}$$

$$F_{AB} = F_{\text{T}} - k_{\text{T}}(d_{\text{T}} + l_{\text{SMA}} - l_{AB}), \text{ where } (l_{\text{SMA}} + d_{\text{T}})$$
$$\leqslant l_{\text{AB}} < (l_{\text{SMA}} + d_{\text{DM}}) \tag{6}$$

$$F_{AB} = F_{\text{DM}} - k_{\text{DM}}(d_{\text{DM}} + l_{\text{SMA}} - l_{AB}),$$
$$\text{where } (l_{\text{SMA}} + d_{\text{DM}}) \leqslant l_{AB} \tag{7}$$

where k_{M}, k_{T} and k_{DM} are the stiffness constants for the twinned martensitic state, transition state and DM, respectively, while F_{T}, d_{T}, F_{DM} and d_{DM} represent the force (F) and displacement (d) thresholds required to switch from the first to second state (equations (5)–(6)) and the second to third state (equations (6)–(7)). These three lines represent the force-displacement behaviour of the martensitic SMA in the twinned, transition and detwinned state respectively and are valid within the limits defined in the equations.

This approach to modelling the force-displacement of martensitic SMA is identical to the analytical method employed previously by the same authors to model uni-axial bias actuator behaviour [14] and is analogous to the Souza-Auricchio numerical method [49, 50] used in many commercial Finite Element software. The equations are expressed in terms of stiffness constants, transformation displacements and forces rather than Young's moduli, strains and stresses in order to ensure that these equations may be applied to an SMA component in any form, be it as a wire, strip, spring or even more complex geometric forms. In the case of SMA wires, as used in the experimental part of this work, these terms may easily be derived directly from basic stress–strain plots, while for other forms less straightforward analytical expressions may be required to obtain these constants. In a similar vein, the austenitic force-displacement behaviour (indicated in figure 3 by the red line) is represented by the following linear model:

$$F_{AB} = k_A(l_{AB} - l_{\text{SMA}}) \tag{8}$$

where k_A represents the stiffness constant of the SMA in its austenitic phase.

On the other hand, as shown in figure 3, the force-displacement behaviour of the bias component counteracting the SMA is represented by a non-linear model along the line AB. This is due to the fact that although the stiffness of the bias component *per se* is constant, it is aligned along the line CD, orthogonal to the line AB. This means that the force component exerted along the line AB as a result of the elongation of the bias component varies non-linearly as a function of the initial configuration of the rotating square metamaterial as shown in figure 4(c).

The force-displacement relationship along the line *CD* for the elastic bias component may be defined by equation (9):

$$F_{CD} = k_E(l_{CD} - l_E) \tag{9}$$

where l_E is the initial length of the elastic bias component and k_E is the associated stiffness constant (see figure 4(a)). This equation can be used to find the resultant force and displacement acting along the line AB through the following kinematic and geometric relationships (shown in figure 4(b)):

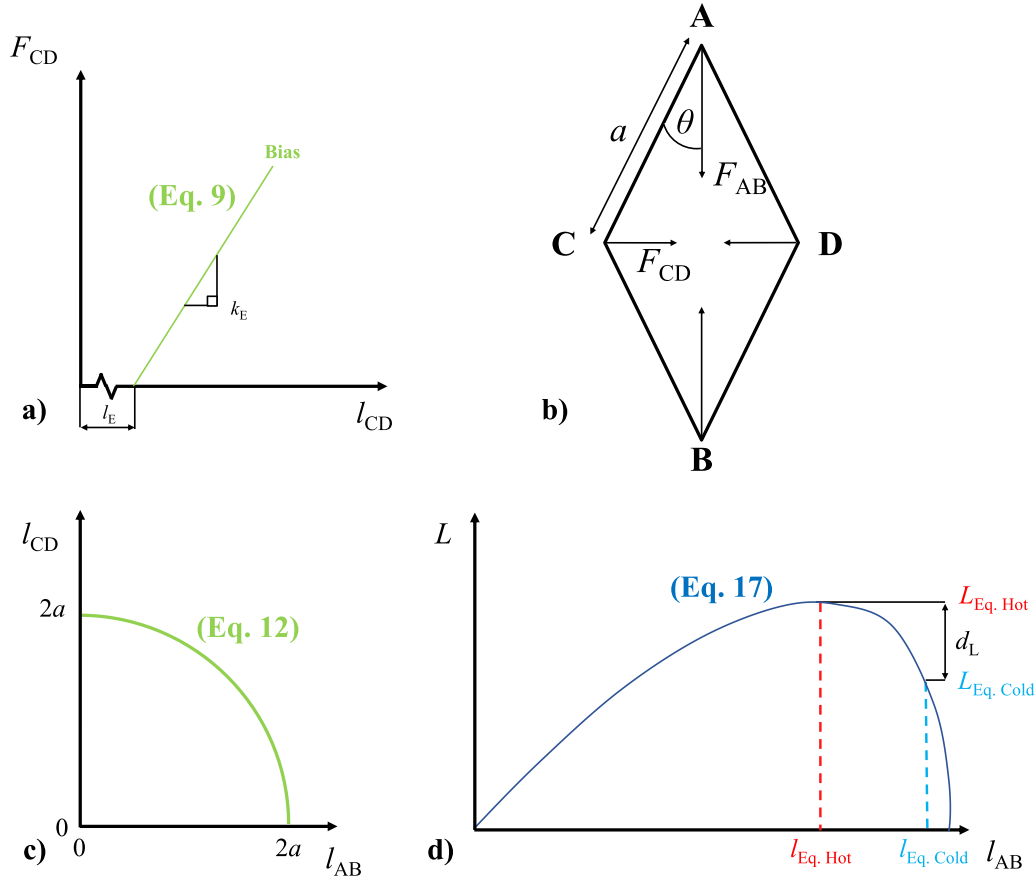$$F_{AB} = \frac{F_{CD}}{\tan \theta} \tag{10}$$

Figure 4. (a) A qualitative plot showing the linear force-displacement model used to describe the deformation of the elastic bias component along the line between points C and D. (b) A diagram showing the forces (F_{AB} and F_{CD}) acting along the directions l_{AB} and l_{CD} in the central pore between the rotating square units. (c) A plot showing the relationship between changes in the lengths l_{AB} and l_{CD} and (d) a graph showing the relationship between overall actuator length in axial and transverse direction, L, and the internal length parameter l_{AB}.

$$\theta = \arccos\left(\frac{l_{AB}}{2a}\right) \tag{11}$$

$$l_{CD} = \sqrt{4a^2 - l_{AB}^2} \tag{12}$$

which in turn can be used to obtain the following non-linear model for the bias component along the line AB (shown in figure 3):

$$F_{AB} = \frac{k_E\left(\sqrt{4a^2 - l_{AB}^2} - l_E\right)}{\tan\left(\arccos\left[\frac{l_{AB}}{2a}\right]\right)} \tag{13}$$

The cold equilibrium point, shown in figure 3, is the point at which the force exerted by the martensitic SMA component and the counteracting elastic bias component are equal. Ideally this point should be met at the DM of the SMA component in order to ensure that the actuation stroke is completely recovered once the actuator is deactivated as demonstrated in [14]. Therefore, the resultant length at the cold equilibrium point, $l_{AB\ Eq.C}$, may be found by solving equations (7) and (13). Once the SMA component is heated and undergoes a reverse transformation, this equilibrium point shifts to the point where equations (8) and (13) are equal. By solving these

two equations, one may find the resultant length at the hot equilibrium point, $l_{AB\ Eq.H}$.

Once the lengths l_{AB} of the actuator when the SMA is in its martensitic and austenitic phase, $l_{AB\ Eq.C}$ and $l_{AB\ Eq.H}$, are known, these variables can be used to find the corresponding cold and hot equilibrium global lengths of the actuator, $L_{Eq.C}$ and $L_{EQ.H}$ (shown in figure 4(b)), through equations (14) and (15):

$$L_{Eq.Cold} = l_{AB\_Eq.Cold} + \sqrt{4a^2 - l_{AB\_Eq.Cold}^2} \tag{14}$$

$$L_{Eq.Hot} = l_{AB\_Eq.Hot} + \sqrt{4a^2 - l_{AB\_Eq.Hot}^2} \tag{15}$$

These equations define the relationship between the contraction of the SMA wire and the global metamaterial geometry and are obtained through the expansion of the generic equation (1). The difference between these two values results in the predicted global actuation stroke in the axial and transverse directions, d_L, as follows:

$$d_L = L_{Eq.Hot} - L_{Eq.Cold} \tag{16}$$

Due to the nonlinearity of the relationship between L and l_{AB} (equation (17)), shown in figure 4(d), it is evident that in order

to obtain the maximum actuation stroke, dl, $l_{AB \text{ Eq.Cold}}$, should ideally be close to the maximum permissible value of l_{AB}, i.e. $l_{AB} \to 2a$. This means that the initial configuration of the rotating squares metamaterials should ideally be at a θ value close to 0°. Yet, it is also important to note that one must be careful to ensure that the initial length of the SMA component, l_{SMA}, is not equal or almost equal to $2a$ since this would entail that the bias component cannot exert any meaningful pre-stress on the wire due to the rotating squares mechanism being blocked in its fully-opened state. Thus, the initial length of the SMA component which allows one to obtain the maximum permissible actuation for a given bias component must first be found through the analytical model.

$$L = l_{AB} + \sqrt{4a^2 - l_{AB}^2} \qquad (17)$$

To summarise, the model presented in this section demonstrates how the actuation stroke of the metamaterial actuator may be predicted and tailored as a function of metamaterial configuration and material properties of the SMA and bias components.

4. Experimental methodology

Bearing in mind the insights obtained from the theoretical model described in the previous section, we designed a prototype actuator based on this concept which is able to impart a global biaxial actuation. As detailed in the following sections, the metamaterial was printed using a fused-deposition method (FDM) 3D printer as four separate parts and assembled using commercially bought components. The SMA component was integrated within the system in the form of a thin wire attached between points A and B and was heated by passing through an electric current from a power supply while the bias mechanism was incorporated through the insertion of a number of elastic bands at points C and D of the actuator in order to counter the contraction of the SMA wire upon heating.

4.1. Thermo-mechanical characterization of the SMA wire

A Nitinol shape-memory wire with a diameter of 0.23 mm was used in this work. The chemical composition of the wire as provided by the supplier is presented in table 1. A thicker sample of wire (diameter 0.43 mm) with the same chemical composition was previously characterised by Panciroli [52] and it was found that the wire has a martensitic finish transformation temperature of 40 °C (315 K) and an austenitic finish transformation temperature of 79 °C (353 K). In order to characterise the force-displacement and stress–strain behaviour of this wire at complete martensitic and austenitic phases, a sample was subjected to tensile loading using Galdabini® tensiometer. The wire was affixed to screws from both ends and trapped using two nuts. The screws were then inserted into two acrilonitrile butadiene stirene (ABS) 3D-printed holders which are clamped by the jaws of the tensile loading machine as shown in figure 5(a).

The wire sample tested had an effective length of 206 mm and was tested at room temperature and under heated

Table 1. Percentage chemical composition of Nitinol wire [52].

Ni	Co	Cu	Cr	Fe
55.42	0.005	0.005	0.005	0.005
Nb	C	H	O	Ti
0.025	0.037	0.001	0.033	44.46

conditions (i.e. at complete martensite and austenite phases respectively). The wire was subjected to a two-step loading and unloading cycle. For the martensitic test, a tensile elongation of 24 mm at a speed of 6 mm min^{-1} was applied followed by a return to the initial position at the same speed. The samples were pre-heated and allowed to cool gradually before initiating the test in order to ensure that any pre-strain applied to the wire during the clamping process was removed. For the austenitic test, a smaller tensile elongation was applied and the wire was heated by the Joule effect throughout the duration of the entire loading and unloading procedure. This was done by connecting a power supply to the screws to which the SMA wire was affixed and applying a current of 0.75 A. In order to ensure that the applied current is sufficient to induce an austenitic transformation, the resistivity of the wire was measured prior to the tensile test at low and high ranges of current and was found to be 8.92×10^{-7} Ωm and 6.36×10^{-7} Ωm, respectively. These values are comparable with those found in the literature for martensitic and austenitic nitinol wires [53]. Once the test sample is mounted, the ABS 3D-printed holders ensure that the wire is isolated from the metallic clamps of the tensile loading machine and that the current heats up the wire. The following stress–strain graph, shown in figure 5(b), was obtained following data smoothening procedures to eliminate minor noise in the data points.

4.2. Additive manufacturing and assembly of the SMA-metamaterial actuator

The rotating square metamaterial structure was designed to function as a single unit cell pin-joint system with minimal stiffness. The four identical square units making up the system were designed using Solidworks® (see figures 6(a), (b) and (g)) and additively-manufactured from Onyx® material using a Markforged® FDM 3D-printer. These square units were designed with an effective side length, a, of 70 mm and an out-of-plane thickness of 20 mm. In order to lower the mass of the squares and avoid unnecessary waste of material, the squares were designed as thick truss systems with a cross pattern, which ensures that the squares retain their rigidity whilst minimising the volume of printing material used [54]. The base metamaterial system was then assembled with the addition of metal commercially-bought hinges (see figure 6(d)) which were attached to the square units through screws, positioned at points A and B shown in figure 6(e). On the other hand, the squares were connected at points C and D through the 3D printed pin-joints shown in figure 6(f). In order to support the actuator on a surface without influencing its in-plane deformation, spherical rolling bearings were attached to the centre of each of the four rotating square units (see figure 6(c)).
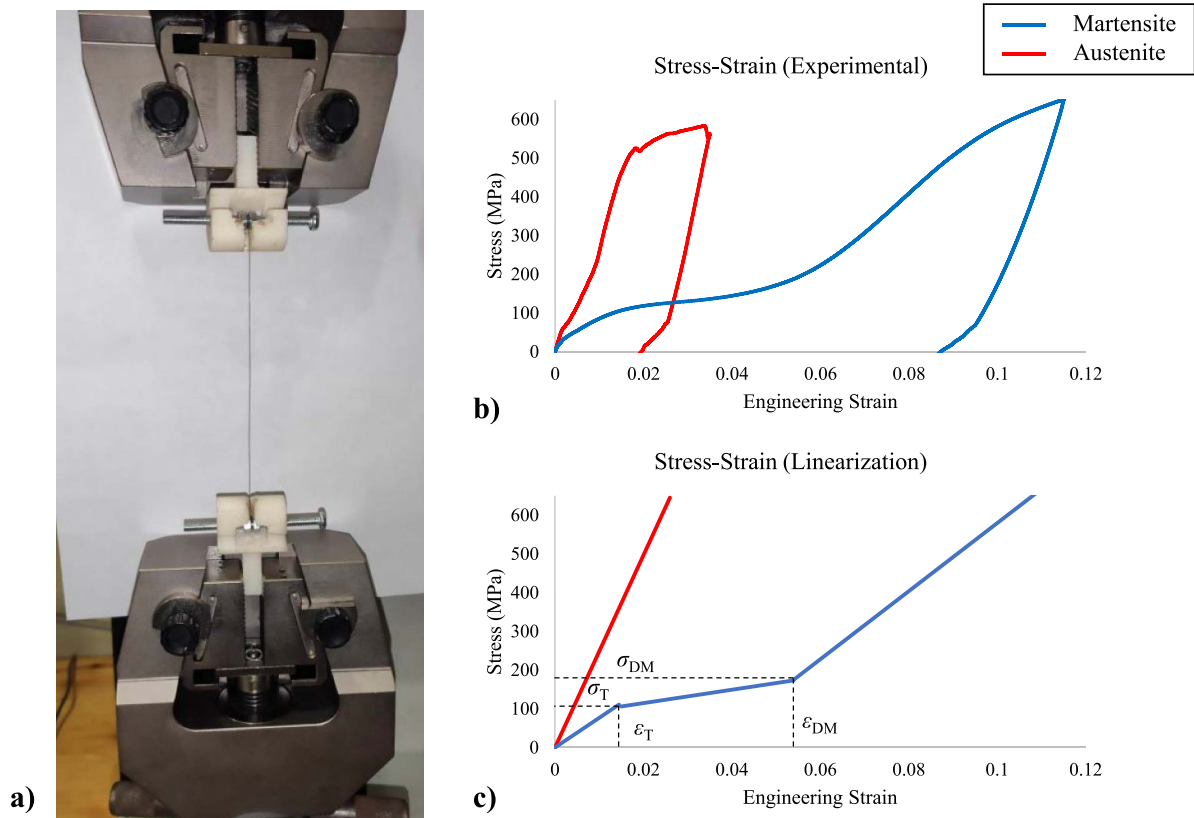
Figure 5. (a) Image showing how the SMA wire was set up for the tensile loading test. (b) Stress–strain plot of the SMA wire in martensitic and austenitic state and (c) linearization of the experimental plot used to obtain the parameters implemented in the theoretical model (see table 3).

Lastly, the joints (both plastic and metallic) and spherical bearings were all lubricated with machine grease in order to minimise friction.

A length of SMA wire was inserted into the actuator by attaching it to points A and B through the use of knots. The initial length of the wire used varied between different experimental runs, but in each case, it was chosen on the basis of resulting in a metamaterial configuration which has a θ value between 10° and 20°. The latter limit ensures that the inverse relationship between lengths l_{AB} and L is retained while the former guarantees that the level of pre-strain imparted by the bias mechanisms to the SMA wire does not result in the length l_{AB} surpassing the mechanical limit of $l_{AB}/a = 2.828$ which is equivalent to a geometrically unrealisable $\theta < 0°$ value. Moreover, in order to ensure that any slippage of the wire during experimental testing is detected, the original length of the wire was marked with white corrective fluid after pre-heating it to eliminate any pre-strain applied during the assembly process. Following the insertion of the SMA, the bias component was added to the system in the form of elastic rubber bands attached to the protruding screws in positions C and D. The rubber bands (with an initial length, l_E, of 25 mm) were tested under tensile loading conditions using an extensometer and were found to have an average linear stiffness of 0.1 MPa over a strain range of 0% to 160%. The system was then allowed to equilibrate before proceeding with the actuation tests. In order

to activate the actuator by heating up the SMA component, a power supply was used and, following preliminary testing, it was found that a current of 1 A for a time period of 10 s was sufficient to guarantee that the wire reached its complete austenitic transformation. The power supply was connected to the actuator by soldering the wire to the metal hinges as shown in figure 6(e) rather than directly to the SMA wire, in order to ensure that the connections do not interfere with the deformation of the actuator.

4.3. Experimental test runs

Three experimental runs were conducted in order to verify the functionality of the prototype SMA-metamaterial actuator. In the first test, a single elastic rubber band was used as a bias mechanism, in the second, two, and, lastly, in the third, three. The initial length of the SMA wire, l_{SMA}, for each test is listed in table 2. In each testing run, the actuator was activated and deactivated 10 times in a row in order to analyse the reversibility of actuation stroke and reusability of the actuator. This was done through sequential 10 s of activation (with a current of 1 A from a power supply) followed by 60 s of deactivation in order to allow the SMA wire to cool and return completely to its martensitic state. The deformation of the actuator was captured through the use of a digital camera (Nikon®) with a frame rate of 5 Hz. Using image correlation techniques, points
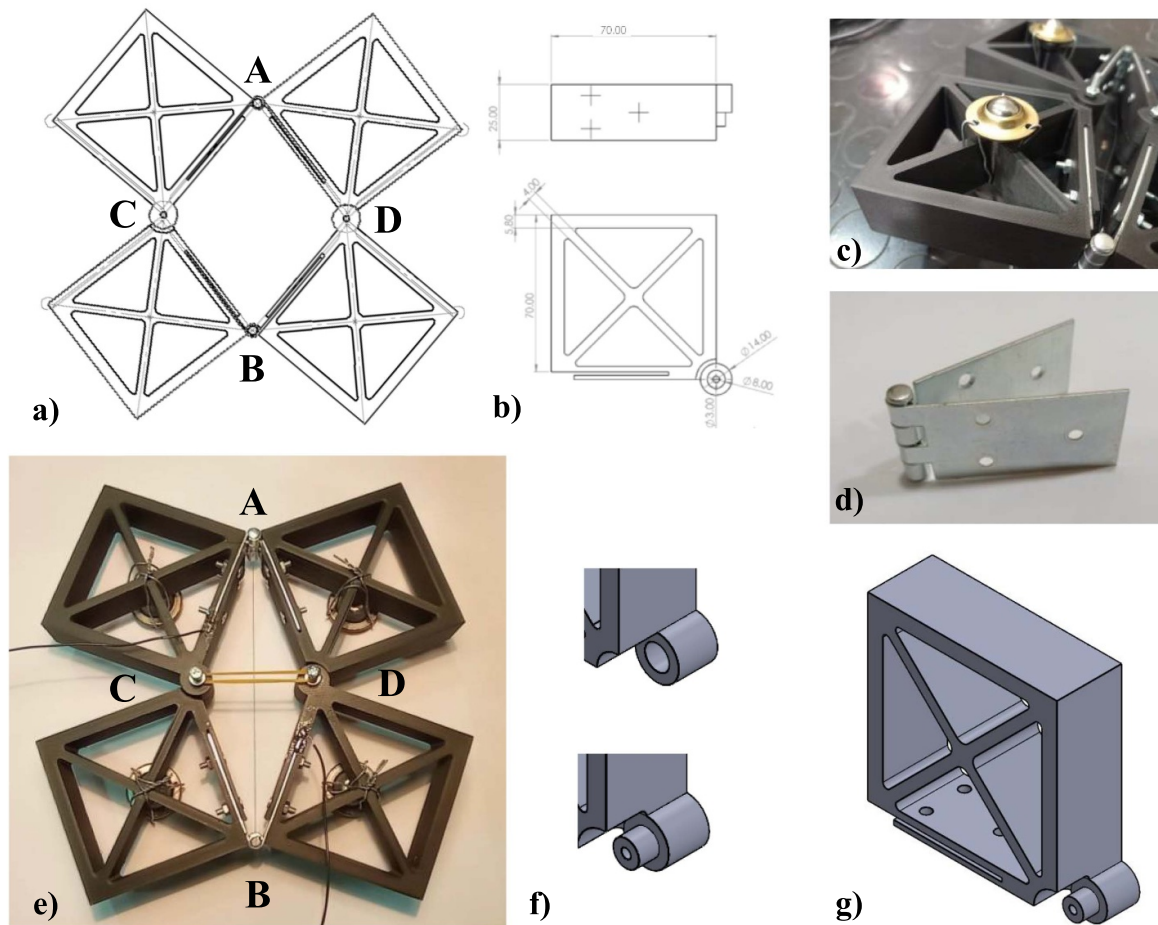
Figure 6. Technical drawing of (a) assembled and (b) individual rotating square units making up the actuator. (c) Spherical bearings used to minimise friction between supporting surface and actuator and (d) metallic hinges inserted in points A and B of the system. (e) SMA-metamaterial actuator showing the wire inserted between points A and B, the elastic rubber bands (bias mechanism) between points C and D and the wiring connecting the metallic hinges to the power supply. Figures (f) and (g) show a zoomed in version of the joints at points C and D which are jointed together through the insertion of a metal M3 screw.

Table 2. List of parameters for three experimental tests run.

Test Number	No. of Elastic Bands	Initial Length of SMA wire (mm)
I	1	110.2
II	2	111.5
III	3	117.2

A, B, C and D of the actuator along with the external corners of the rotating squares, were tracked in order to obtain the experimental values of l_{AB}, l_{CD} and L throughout each activation and deactivation cycle, as shown in figure 7. The global actuation stroke, d_L, for each cycle was calculated as the difference between the length of L before and after activation.

5. Results and discussion

The resultant global actuation stroke, d_L, obtained for each experimental run with respect to the number of activation/deactivation cycles, along with images of the

actuator in its activated and deactivated states are presented in figure 8. It is clearly evident from the plots that while in Test I the actuation stroke was almost nil, in Test runs II and III, a significant actuation stroke was observed which remained more or less stable over 10 consecutive activation/deactivation cycles, undoubtedly demonstrating both the functionality and reversibility of the prototype actuator. Moreover, as shown in figure 8(a), the actuation stroke is biaxial and the rotation of the square units is plainly visible indicating that the pin-jointed metamaterial structure is indeed deforming as intended.

In order to analyse these results in the context of the predictions of the theoretical model presented in section 3 of this article, it is necessary to first obtain the Young's moduli, E_A, E_M, E_T and E_{DM}, transformation stresses, σ_T and σ_{DM}, and strains, ε_T and ε_{DM}, of the SMA in martensitic and austenitic phase. Utilising linear regression, the following constants, presented in table 3, were obtained from the stress–strain plot shown in figure 5(b).

These terms can be used to obtain the corresponding stiffness constants and transformation forces and displacements necessary to plot the tri-linear martensitic model
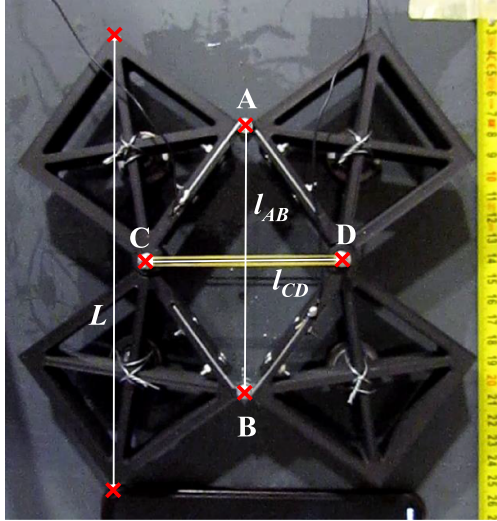
Figure 7. Image showing the points which were tracked using image correlation techniques (marked with a cross) in order to measure lengths l_{AB}, l_{CD} and L.

Table 3. Young's moduli, transformation stresses and strains obtained from the austenitic and martensitic stress–strain plot shown in figure 5(b).

SMA Parameters			
E_A	24 815.14 MPa	ε_T	0.015
E_M	7614.26 MPa	σ_T	106 MPa
E_T	1724.63 MPa	ε_{DM}	0.054
E_{DM}	8790.63 MPa	σ_{DM}	175 MPa

(equation (5)–(7)) and linear austenitic model (equation (8)) as follows:

$$k_A = \frac{E_A A}{l_{SMA}} \tag{18}$$

$$k_M = \frac{E_M A}{l_{SMA}} \tag{19}$$

$$k_T = \frac{E_T A}{l_{SMA}} \tag{20}$$

$$k_{DM} = \frac{E_{DM} A}{l_{SMA}} \tag{21}$$

$$F_T = \sigma_T A \tag{22}$$

$$F_{DM} = \sigma_{DM} A \tag{23}$$

$$d_T = \varepsilon_T l_{SMA} \tag{24}$$

$$d_{DM} = \varepsilon_{DM} l_{SMA} \tag{25}$$

where A is defined as the cross-sectional area of the SMA wire ($\pi d^2/4$) and l_{SMA}, the length of the wire. The initial lengths used for each test are listed in table 2. For the elastic rubber bands, the stiffness constant of a single rubber band, k_R, was

equal to 0.1 MPa and, thus, the stiffness constant used to plot the force/displacement plot of the bias mechanism, k_E, may be found as follows:

$$k_E = N k_R \tag{26}$$

where N is the number of rubber bands used in each test (listed in table 2).

Utilizing these constants, the simultaneous equation pairs: equations (7), (13) and equations (8), (13), were solved numerically in order to obtain the cold and hot equilibrium points, $l_{AB \text{ Eq.C}}$ and $l_{AB \text{ Eq.H}}$, respectively. These values were then used to find the predicted actuation stroke, d_L, for each of the three experimental test runs using equations (14)–(16). These theoretically predicted values are plotted along with the average value of the global actuation stroke obtained from the experimental results in figure 9.

It is evident from figure 9 that while the theoretical model overestimates the experimental actuation stroke, particularly for Tests I and III, the trends obtained using both methods are congruous with each other. The discrepancies in the magnitude of the values were also to be expected since the experimental prototype does not completely conform with all the assumptions used to derive the analytical expressions. For example, the model assumes ideal frictionless rotation of the square units, however some friction is always present despite the lubrication of the joints and the use of spherical bearings. Moreover, the model does not take into account the influence of functional fatigue, which cannot be disregarded completely for actuator configurations where the SMA component is subjected to a high initial level of pre-strains such as in Test III. In view of this, the theoretical model is envisaged to be primarily utilizable as a pre-design tool for the fabrication of SMA-metamaterial actuators since it has the highest accuracy for predicting the initial actuation cycles of the system.

The results obtained from the tests on the metamaterial actuator prototype also provide a number of additional insights on the functionality of this actuator. In the case of Test I, where only one rubber band was used, it was clearly evident that the force generated by this elastic bias component was not sufficient to guarantee a sufficient level of pre-strain to the SMA component in order to allow it to reach its complete DM. This, in turn resulted in an extremely low actuation stroke output (as also predicted by the theoretical model) as well as decreasing the amount of recoverable actuation stroke due to the fact that the cold equilibrium point is reached at the transition phase of the martensitic SMA. This highlights the importance of having a bias component that is capable of generating the necessary level of pre-strain in the SMA component, elsewise the actuation output will be extremely low. However, while increasing the level of pre-strain will give a higher actuation stroke, it is also important to keep in mind that a large pre-strain value will lead to an increase in the fatigue of the SMA component. This results in yielding, and thus a decrease of functionality, occurring at a lower number of actuation cycles. This factor was, in fact, particularly evident in Test III. Although the plot shown in figure 8(b)(iii) indicates an
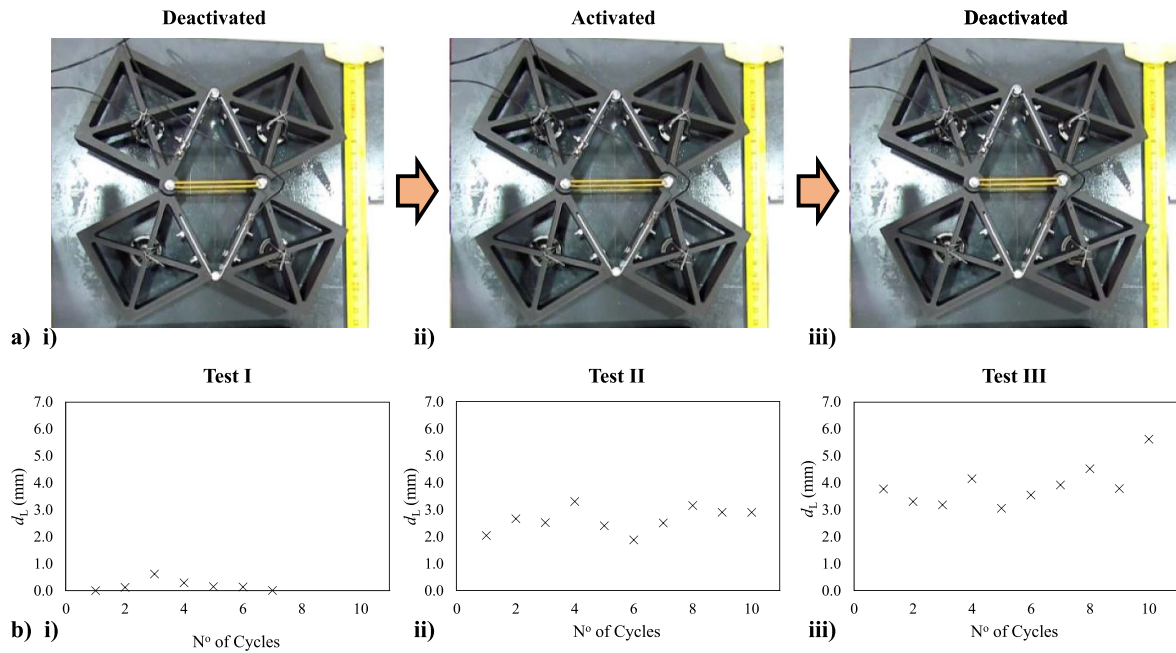
Figure 8. (a) Images showing the second cycle ((i) deactivated actuator, followed by (ii) activation and (iii) deactivation) of the actuator with three elastic rubber bands (Test III) (b) Plots showing the resultant global actuation stroke measured for each activation/deactivation cycle of the three experimental tests listed in table 2. Note, that in Test I, the number of cycles was terminated early due to the fact that almost no actuation stroke was observed over repeated cycles.
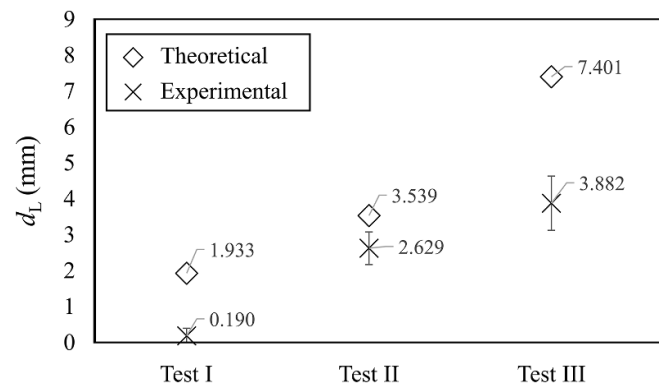

Figure 9. Plot showing the comparison between the theoretical d_L values predicted by the analytical model and the corresponding average experimental values (over 10 cycles) with standard deviation.

almost constant actuation stroke, d_L, throughout the 10 activation/deactivation cycles, a closer analysis of how the absolute value of the global length of the actuator, L, varies with each cycle (see figures 10(a)(ii) and (b)) shows that this value is significantly decreasing after every cycle despite the actuation stroke remaining constant. This indicates that the SMA wire is undergoing irreversible yielding with each cycle due to the high level of pre-strain imposed by the bias mechanism (in this case three rubber bands). This effect is not visible in the Cycle No° vs d_L plot shown in figure 8(b)(iii) due to the fact that the elastic bias mechanism is undergoing a large level of pre-strain itself and thus the actuation stroke lost due to yielding relaxation of the SMA component is re-gained by

the imposition of an additional increment of pre-strain on the wire. This leads to an initial masking of the SMA yielding effect which is advantageous if maintaining a constant actuation stroke is the main function of the actuator, however it is also expected to result in a more rapid deterioration of actuator functionality over time. On the other hand, in the case of Test II, it is clear that the change in L is minimal over 10 cycles and that both the actuation stroke and absolute actuator dimensions remain almost constant (see figure 10(a)(i)). This indicates that out of the three configurations tested, this is the one which shows the best performance since it is characterized by an appreciable actuation stroke while the observed yielding of the SMA component is minimal over 10 cycles.
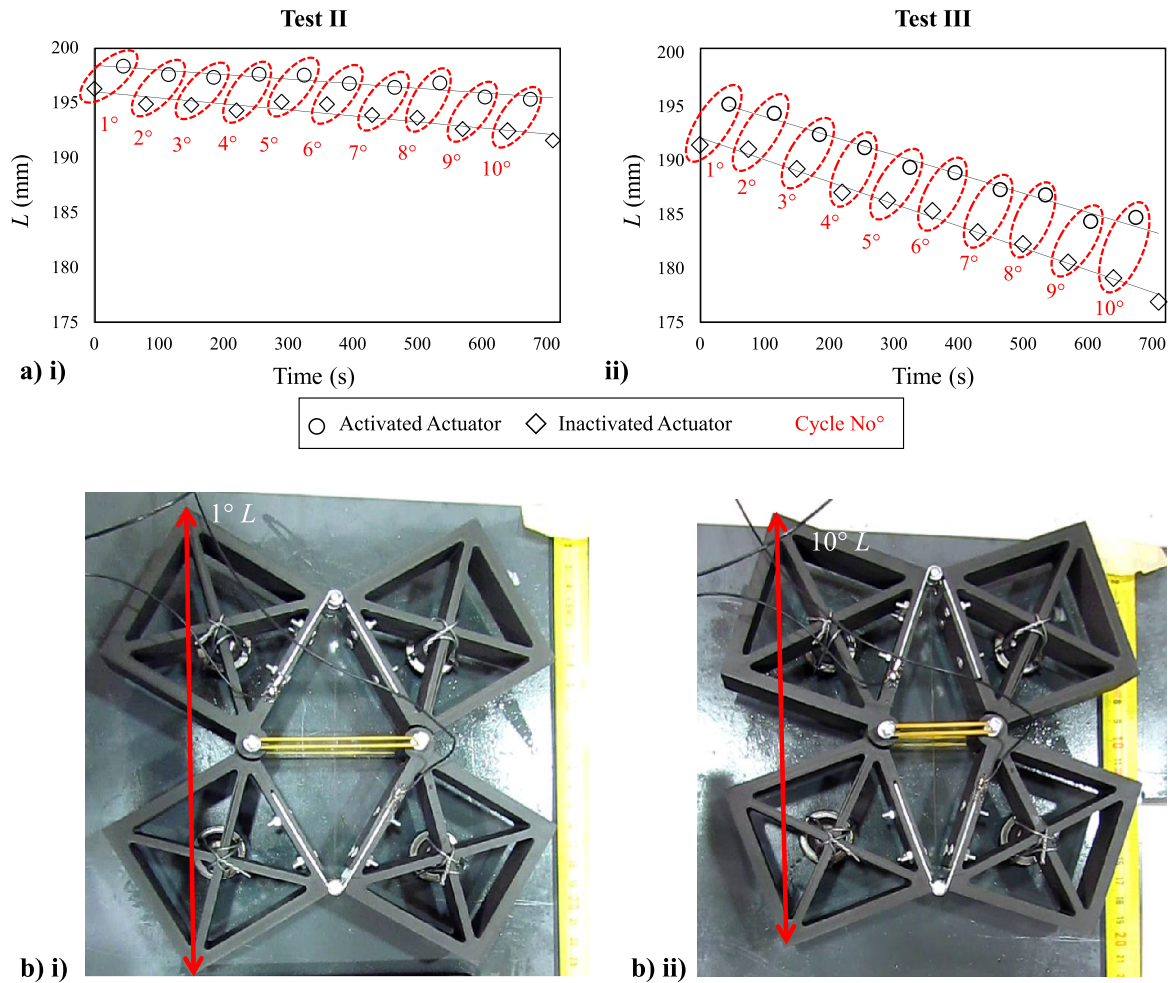
Figure 10. (a) Plots showing how the absolute value of L changes over testing time for (i) Test II and (ii) Test III. The dotted red lines indicate the actuation cycles while the black lines are plotted by linear regression of the actuator in its activated and deactivated state separately in order to roughly indicate how L changes over time. (b) Images showing the difference in the deactivated configuration of the actuator in Test III after (i) the $1°$ cycle and (ii) the $10°$ cycle.

From the insights obtained from the theoretical model and experimental results, it is clear that in order to design an SMA-metamaterial actuator with optimal performance based on the rotating squares mechanism, one should aim to:

- Ensure that the bias mechanism used exerts sufficient force on the SMA component in order to bring it to the highest possible allowable pre-strain value which does not result in irreversible yielding effects. By reaching the optimum equilibrium point one can obtain the highest actuation stroke of the SMA component while minimizing loss of functionality due to fatigue.
- Design the rotating square metamaterial system in such a way as to have an initial configuration at the cold martensitic equilibrium point which has a low θ value. This ensures that the actuation stroke of the SMA component ($L_{\text{Eq.Hot}}-L_{\text{Eq.Cold}}$) is amplified to its maximum level and translates into a large global actuation stroke, d_L.

Before concluding, it is imperative to point out that the SMA-metamaterial actuator proposed and prototyped in this work is merely one example which illustrates the potential of this new class of SMA actuators. The main advantage of using a metamaterial geometry to control the global actuation output of an SMA-based actuator lies in the fact that one can manipulate the deformation of these systems based on geometry. Thus, the designer has a variety of options to choose from when designing these types of actuators in order to obtain a tailored and desired output. For example, the actuator presented in this work, which is designed to exhibit a biaxial positive stroke, can easily be changed into an actuator which delivers a biaxial negative stroke (i.e. overall global contraction) simply by inverting the positions of the SMA wire and bias component, i.e. placing the SMA wire in position CD and the bias mechanism in position AB. Furthermore, the force exerted by the bias mechanism can be tuned simply by changing its placement with respect to the SMA component. By changing the position (such as for example attaching it to the centre of the rotating squares), one can alter the bias force it exerts in counteracting the SMA component and hence one can simply optimize the SMA-bias equilibrium point as a function of bias component positioning rather than by using a different material.

The use of a biaxial actuator which is activated through the uniaxial deformation of a single component such as the one proposed in this work presents various advantages over traditional biaxial actuators powered by separate components for each direction. The most obvious advantage is the reduced risk of unequal actuation in the transverse and axial directions in case of a malfunction. Since the global actuation stroke is induced solely by a single SMA component and is kinematically governed by the metamaterial geometry, the ratio of axial to transverse actuation stroke is fixed by design and cannot physically change while the system is in place. This means that if actuation is blocked in a single direction, then by default it is also obstructed in the orthogonal direction, thus retaining the uniformity of bi-directional actuation. This, in turn, also reduces the need for constant recalibration of the actuator after use, as is the case for biaxial actuators which are driven by separate, independent components for each direction. This property makes metamaterial-based actuators particularly well-suited for potential future use as platforms for biaxial loading testing rigs as well as implementation in deployable structures requiring tailored biaxial actuation.

Finally, it is important to emphasize that while in this work the main aim was to design a reversible actuator capable of producing an equal biaxial actuation stroke and, hence, the auxetic rotating square mechanism with a characteristic Poisson's ratio of -1 was chosen, a plethora of other rotating structures may be found within the literature, which may be used to design similar actuators with different advanced functionalities. For example, certain configurations of the rotating rectangle mechanism are known to have the capability of exhibiting giant negative/positive Poisson's ratios and one may take advantage of this property to simply greatly amplify the actuation stroke of the standalone SMA component in a single direction. On the other hand, if one wishes, for instance, to design an actuator which exhibits an equal tri-axial deformation, rotating systems with trigonal in-plane symmetry such as rotating triangle structures may be used as a basis for such an actuator. All in all, the possibilities for designing and realizing SMA-metamaterial actuators with multi-axial actuation capabilities and geometrically-tailored outputs are nearly endless and we believe that the results presented in this work will give rise to further studies on this interesting class of smart composite structures.

6. Conclusions

In this work, we have designed a new reversible SMA-based actuator with an equal biaxial actuation stroke based on an auxetic metamaterial structure. Through the use of the rotating square system, which is characterized by a Poisson's ratio of -1, the axial uni-directional contraction of the SMA component upon activation is translated into a biaxial global expansion of the overall actuator. An experimental prototype of this actuator was manufactured and assembled and then tested under three different configurations over 10 activation/deactivation cycles. A theoretical model which may be used as a pre-design tool for the realization of SMA-metamaterial actuators with a tailored actuation stroke has also been developed and its predictions compared with the experimental results. This work highlights the potential of SMA-metamaterial actuators for implementation in systems requiring a multi-axial actuation output and we hope that the findings presented in this work will act as a blueprint for the design of other metamaterial-based SMA actuators with advanced functionalities.

Data availability statement

The data that support the findings of this study are available upon reasonable request from the authors.

ORCID iDs

Luke Mizzi ⬚ https://orcid.org/0000-0002-7650-1173
Andrea Spaggiari ⬚ https://orcid.org/0000-0001-8959-2599

References

[1] Lagoudas D C 2008 *Shape Memory Alloys* vol 1 (Boston, MA: Springer)
[2] Mohd Jani J, Leary M, Subic A and Gibson M A 2014 A review of shape memory alloy research, applications and opportunities *Mater. Des.* **56** 1078–113
[3] Sun L, Huang W M, Ding Z, Zhao Y, Wang C C, Purnawali H and Tang C 2012 Stimulus-responsive shape memory materials: a review *Mater. Des.* **33** 577–640
[4] Spaggiari A, Castagnetti D, Golinelli N, Dragoni E and Scire Mammano G 2016 Smart materials: properties, design and mechatronic applications *Proc. Inst. Mech. Eng.* L **0** 1–29
[5] Wang F E, Buehler W J and Pickart S J 1965 Crystal structure and a unique martensitic transition of TiNi *J. Appl. Phys.* **36** 3232–9
[6] Ford D S and White S R 1996 Thermomechanical behaviour of 55Ni45Ti Nitinol *Acta Mater.* **44** 2295–307
[7] Mahtabi M J, Shamsaei N and Mitchell M R 2015 Fatigue of Nitinol: the state-of-the-art and ongoing challenges *J. Mech. Behav. Biomed. Mater.* **50** 228–54
[8] Robertson S W, Pelton A R and Ritchie R O 2012 Mechanical fatigue and fracture of Nitinol *Int. Mater. Rev.* **57** 1–37
[9] Pelton A R 2011 Nitinol fatigue: a review of microstructures and mechanisms *J. Mater. Eng. Perform.* **20** 613–7
[10] Ishii H and Ting K L 2004 SMA actuated compliant bistable mechanisms *Mechatronics* **14** 421–37
[11] Reynaerts D and Van Brussel H 1998 Design aspects of shape memory actuators *Mechatronics* **8** 635–56
[12] Nespoli A, Besseghini S, Pittaccio S, Villa E and Viscuso S 2010 The high potential of shape memory alloys in developing miniature mechanical devices: a review on shape memory alloy mini-actuators *Sens. Actuators* A **158** 149–60
[13] Spaggiari A, Scirè Mammano G and Dragoni E 2012 Optimum mechanical design of binary actuators based on shape memory alloys *Smart Actuation Sens Syst—Recent Adv Futur Challenges* (Croatia: Intech Publ) ch 1, pp 3–34
[14] Mizzi L, Spaggiari A and Dragoni E 2019 Design-oriented modelling of composite actuators with embedded shape memory alloy *Compos. Struct.* **213** 37–46
[15] Rao A, Srinivasa A R and Reddy J N 2015 *Design of Shape Memory Alloy (SMA) Actuators*
[16] Ghosh P, Rao A and Srinivasa A R 2013 Design of multi-state and smart-bias components using shape memory alloy and shape memory polymer composites *Mater. Des.* **44** 164–71

[17] Spaggiari A and Dragoni E 2014 Analytical and numerical modeling of shape memory alloy Negator springs for constant-force, long-stroke actuators *J. Intell. Mater. Syst. Struct.* **25** 1139–48

[18] John S and Hariri M 2008 Effect of shape memory alloy actuation on the dynamic response of polymeric composite plates *Composites* A **39** 769–76

[19] Quade D, Jana S, Morscher G, Kannan M and McCorkle L 2018 The effects of fiber orientation and adhesives on tensile properties of carbon fiber reinforced polymer matrix composite with embedded nickel-titanium shape memory alloys *Composites* A **114** 269–77

[20] Bettini P, Riva M, Sala G, Di Landro L, Airoldi A and Cucco J 2009 Carbon fiber reinforced smart laminates with embedded SMA actuators-part I: embedding techniques and interface analysis *J. Mater. Eng. Perform.* **18** 664–71

[21] Simoneau C, Terriault P, Lacasse S and Brailovski V 2014 Adaptive composite panel with embedded SMA actuators: modeling and validation *Mech. Based Des. Struct. Mach.* **42** 174–92

[22] Renata C, Huang W M, He L W and Yang J J 2017 Shape change/memory actuators based on shape memory materials *J. Mech. Sci. Technol.* **31** 4863–73

[23] Pappada S, Gren P, Tatar K, Gustafson T, Rametta R, Rossini E and Maffezzoli A 2009 Mechanical and vibration characteristics of laminated composite plates embedding shape memory alloy superelastic wires *J. Mater. Eng. Perform.* **18** 531–7

[24] Scirè Mammano G and Dragoni E 2011 Increasing stroke and output force of linear shape memory actuators by elastic compensation *Mechatronics* **21** 570–80

[25] Viet N V and Zaki W 2019 Bending model for a laminated composite cantilever beam with multiple embedded shape memory alloy layers presenting tensile compressive asymmetry *Compos. Struct.* **1** 111410

[26] Dezaki M L, Bodaghi M, Serjouei A, Afazov S and Zolfagharian A 2022 Adaptive reversibile composite-based shape memory alloy soft actuators *Sens. Actuators* A **345** 113779

[27] Zadeh M N, Garrad M, Romero C, Conn A, Scarpa F and Rossiter J 2022 RoboHeart: a bi-directional zipping actuator *IEEE Robot. Autom. Lett.* **7** 10352–8

[28] Lu Z K and Weng G J 2000 A two-level micromechanical theory for a shape-memory alloy reinforced composite *Int. J. Plast.* **16** 1289–307

[29] Cho H K and Rhee J 2012 Nonlinear finite element analysis of shape memory alloy (SMA) wire reinforced hybrid laminate composite shells *Int. J. Non-Linear Mech.* **47** 672–8

[30] Birman V 1997 Stability of functionally graded shape memory alloy sandwich panels *Smart Mater. Struct.* **6** 278–86

[31] Ghaznavi A and Shariyat M 2017 Non-linear layerwise dynamic response analysis of sandwich plates with soft auxetic cores and embedded SMA wires experiencing cyclic loadings *Compos. Struct.* **171** 185–97

[32] Khalili S M R, Dehkordi M B, Carrera E and Shariyat M 2013 Non-linear dynamic analysis of a sandwich beam with pseudoelastic SMA hybrid composite faces based on higher order finite element theory *Compos. Struct.* **96** 243–55

[33] Mizzi L, Spaggiari A and Dragoni E 2020 Design of shape memory alloy sandwich actuators: an analytical and numerical modelling approach *Smart Mater. Struct.* **29** 085027

[34] Dehkordi M B and Khalili S M R 2015 Frequency analysis of sandwich plate with active SMA hybrid composite face-sheets and temperature dependent flexible core *Compos. Struct.* **123** 408–19

[35] Grima J N and Evans K E 2000 Auxetic behavior from rotating squares *J. Mater. Sci. Lett.* **19** 1563–5

[36] Grima J N, Alderson A and Evans K E 2004 Negative Poisson's ratios from rotating rectangles *J. Comput. Methods Sci. Eng.* **10** 137–45

[37] Grima J N, Gatt R, Alderson A and Evans K E 2005 On the auxetic properties of 'rotating rectangles' with different connectivity *J. Phys. Soc. Japan* **74** 2866–7

[38] Attard D and Grima J N 2008 Auxetic behaviour from rotating rhombi *Phys. Status Solidi* **245** 2395–404

[39] Attard D, Manicaro E and Grima J N 2009 On rotating rigid parallelograms and their potential for exhibiting auxetic behaviour *Phys. Status Solidi* b **2044** 2033–44

[40] Mizzi L, Azzopardi K M, Attard D, Grima J N and Gatt R 2015 Auxetic metamaterials exhibiting giant negative Poisson's ratios *Phys. Status Solidi* **9** 425–30

[41] Grima J N and Evans K E 2006 Auxetic behavior from rotating triangles *J. Mater. Sci.* **1** 3193–6

[42] Grima J N, Chetcuti E, Manicaro E, Attard D, Gatt R and Evans K E 2012 On the auxetic properties of generic rotating rigid triangles *Proc. R. Soc.* A **468** 810–30

[43] Attard D and Grima J N 2012 A three-dimensional rotating rigid units network exhibiting negative Poisson's ratios *Phys. Status Solidi* **249** 1330–8

[44] Ren X, Shen J, Ghaedizadeh A, Tian H and Xie Y M 2015 Experiments and parametric studies on 3D metallic auxetic metamaterials with tuneable mechanical properties *Smart Mater. Struct.* **24** 095016

[45] Bertoldi B K, Reis P M, Willshaw S and Mullin T 2009 Negative poisson's ratio behavior induced by an elastic instability *Adv. Funct. Mater.* **22** 1–6

[46] Taylor M, Francesconi L, Gerendás M, Shanian A and Carson C 2013 Low porosity metallic periodic structures with negative Poisson's ratio Adv. Mater. **26** 2365–70

[47] Mizzi L, Gatt R and Grima J N 2015 Non-porous grooved single-material auxetics *Phys. Status Solidi* b **252** 1559–64

[48] Mizzi L, Salvati E, Spaggiari A, Tan J and Korsunsky A M 2020 2D auxetic metamaterials with tuneable micro-/nanoscale apertures *Appl. Mater. Today* **20** 100780

[49] Souza A C, Mamiya E N and Zouain N 1998 Three-dimensional model for solids undergoing stress-induced phase transformations *Eur. J. Mech.* A **17** 789–806

[50] Auricchio F and Petrini L 2002 Improvements and algorithmical considerations on a recent three-dimensional model describing stress-induced solid phase transformations *Int. J. Numer. Methods Eng.* **55** 1255–84

[51] Auricchio F and Petrini L 2004 A three-dimensional model describing stress-temperature induced solid phase transformations: solution algorithm and boundary value problems *Int. J. Numer. Methods Eng.* **61** 807–36

[52] Panciroli R 2020 Influence of electric current on the thermo-mechanical static and fatigue properties of shape memory NiTi wires *Smart Mater. Struct.* **29** 115046

[53] Cho H, Yamamoto T, Takeda Y, Suzuki A and Sakuma T 2010 Exploitation of shape memory alloy actuator using resistance feedback control and its development *Prog. Nat. Sci. Mater. Int.* **20** 97–103

[54] Mizzi L and Spaggiari A 2020 Lightweight mechanical metamaterials designed using hierarchical truss elements *Smart Mater. Struct.* **29** 105036